Bearing signal separation enhancement with application to helicopter transmission system

Elasha, F, Mba, D & Greaves, M

Original citation & hyperlink:
Elasha, F, Mba, D & Greaves, M 2017, 'Bearing signal separation enhancement with application to helicopter transmission system' *Journal of Aerospace Engineering*, vol 30, no. 5
https://dx.doi.org/10.1061/(ASCE)AS.1943-5525.0000744

DOI 10.1061/(ASCE)AS.1943-5525.0000744
ISSN 0893-1321
ESSN 1943-5525

Publisher: American Society of Civil Engineers

Bearing signal separation enhancement with application to a helicopter transmission system

Faris Elasha[1*], Matthew Greaves[2], David Mba[3]

[1] Lecturer, Faculty of Engineering, Environment and computing, Coventry University, Gulson Road, Coventry, CV1 2JH (UK). Email :faris.elasha@coventry.ac.uk

[2] Senior Lecturer, School of Aerospace, Transport, and Manufacturing, Cranfield University, College Road, Bedfordshire, MK43 0AL (UK), Email: m.j.greaves@cranfield.ac.uk

[3] Faculty of Technology, De Montford Univsity., Leicester LE1 9BH, U.K.
Email: david.mba@dmu.ac.uk.

Abstract

Bearing vibration signal separation is essential for fault detection of gearboxes, especially where the vibration is nonstationary, susceptible to background noise, and subjected to an arduous transmission path from the source to the receiver. This paper presents a methodology for improving fault detection via a series of vibration signal processing techniques, including signal separation, synchronous averaging (SA), spectral kurtosis (SK), and envelope analysis. These techniques have been tested on experimentally obtained vibration data acquired from the transmission system of a CS-29 Category A helicopter gearbox operating under different bearing damage conditions. Results showed successful enhancement of bearing fault detection on the second planetary stage of the gearbox

1 Introduction

Many diagnosis techniques have been employed for gearbox diagnostics, however, vibration analysis emerged as one of the best diagnosis techniques (Cotrell 2002, McFadden 1987, Samuel, Pines 2005, McFadden, Toozhy 2000, Wang 2001, Sawalhi, Randall et al. 2014). Bearing fault detection within transmission system is one of difficult diagnosis tasks, resulting from the influence of bearing signal transmission from the source to the accelerometer fixed to the external casing. As consequence, the bearing signal will be dominated by other strong components of the vibration signal such as gear meshing. (McFadden 1987, McFadden, Toozhy 2000, McFadden, Smith 1984).

Early attempts utilised time domain averaging to separate the gear components from the measured vibration signal in order to reduce the signal-to-noise ratio (SNR). This involves combining a delayed version of the measured vibration signal with the original signal thereby reinforcing certain frequency components, whilst eliminating others. However, the signal to noise ratio (SNR) enhancement with this technique is not always sufficient to aid detection of bearing faults and hence this technique has not proved successful in identifying bearing defects within planetary gearboxes (McFadden 1987). Time Synchronous Averaging (TSA) has also been applied to separate the bearing vibration components from the measured gearbox signature (McFadden, Toozhy 2000, Yang, Tavner et al. 2009, Wenxian Yang, Tavner et al. 2010, Randall, Sawalhi et al. 2011, Randall, Antoni 2011). This minimises the influence of speed variation by re-sampling the signal in the angular domain (McFadden, Toozhy 2000). The process of re-sampling the signal requires a tachometer or phase marker and is not commonly applied for the sole purpose of separating the bearing vibration signature (Randall, Sawalhi et al. 2011).

Methods such as linear prediction, signal noise cancellation and autoregressive have been used to achieve signal separation. However, such methods are adequate for the stationary signal.(Randall, Sawalhi et al. 2011, Antoni, Randall 2001, Randall 2004, Ho, Randall 2000). Many alternative techniques have been suggested to separate

signals under non-stationary condition (Randall, Sawalhi et al. 2011, Antoni 2005, Li, Yan et al. 2013, Barszcz 2009). Which present most of the vibration signals acquired from gearboxes (Randall 2011, Wang 2008). The performance of these techniques varies depend on the signal history length. The shorter signal history results in a poor prediction, and as consequence, the separated signal will be dominated by strong signal component. However, this will lead to short processing time(Makhoul 1975, Satorius, Zeidler et al. 1979).

To overcome the problem of separation of non-stationary vibrations, adaptive filters were proposed. This concept is based on the Wold Theorem, in which the signal can be decomposed into deterministic and non-deterministic parts. It has been applied to signal processing in telecommunication (Satorius, Zeidler et al. 1979) and Electrocardiography ECG signal processing (Thakor, Zhu 1991). The separation is based on the fact that the deterministic part has a longer correlation than the random part and therefore the autocorrelation is used to distinguish the deterministic part from the random part. However, a reference signal is required to perform the separation. The application of this theory in condition monitoring was established by Chaturvedi et al. (Chaturved, Thomas 1981) where the Adaptive Noise Cancellation (ANC) algorithm was applied to separate bearing vibrations corrupted by engine noise, with the bearing vibration signature used as a reference signal for the separation process. However, for practical diagnostics, the reference signal is not always readily available. As an alternative, a delayed version of the signal has been proposed as a reference signal and this method is known as self-adaptive noise cancellation (SANC) (Ho, Randall 2000) which is based on delaying the signal until the noise correlation is diminished and only the deterministic part is correlated (Antoni, Randall 2001).

Many recursive algorithms have been developed specifically for adaptive filters (Antoni, Randall 2004, Widrow, Glover et al. 1975). Each algorithm offers its own features and therefore the algorithm to be employed should be selected carefully depending on the signal under consideration. Selection of the appropriate algorithm is determined by many factors, including convergence, type of signal (stationary or non-stationary) and accuracy (Simon 1991).

The Spectral Kurtosis technique has been introduced recently for bearing signal separation (Ruiz-Cárcel, Hernani-Ros et al. 2014, Antoni, Randall 2006). In which the kurtosis of decomposed signals is estimated and the signal with higher kurtosis present the impacts due to the bearing fault. Such method depends on the decomposition method.(Antoni 2007), therefore Antoni et al has suggested a methodology known as Fast Kurtogram, and it is based on calculating the kurtosis for all possible frequency bands (Antoni 2007). Dwyer et al have developed the Spectral Kurtosis (SK) (Dwyer 1983) to detect the frequency band of the random component of a signal. Therefore this method employed to extract the transient in the bearing signal and perform the demodulation analysis (Antoni, Randall 2006).

Most of the recent research has focused most on developing a single method to separate bearing signal, therefore this paper proposes improving signal separation through a combination of synchronous averaging and adaptive filters. For this purpose vibration data collected from a CS-29 category 'A' was used for detect bearing fault in the epicyclic module. Vibration signals have been collected under different bearing fault severity, the vibration signals have processed with a set of signal processing techniques such as adaptive filter, time synchronous and envelope analysis.

1. Signal Separation algorithms

In order to compare the effect of employing TSA for improving signal separation, vibration signals acquired were processed using two different paths. For the first path, Deterministic vibration signal has been determined by the means of adaptive filter. Then the SK algorithm has been employed to determine the optimum filter used for demodulation. Finally, Fast Fourier Transform FFT has been used to obtain the demodulated signal spectrum, the signal processing procedures are summarised in figure 1. Synchronous averaging (SA) has been performed by resampling the vibration data in the angular domain (to remove the speed fluctuation) followed by adaptive filtering to separate the random component of the data (bearing signal).The signal separation was performed with an adaptive filter using fast block algorithm least mean square algorithm FBLMS described by Elasha et. al (Elasha, Ruiz-Carcel et al. 2014).

The Fast Block LMS (FBLMS) algorithm was proposed to reduce the processing time (Dentino, McCool et al. 1978) and as such is more suitable for online diagnostics where an instantaneous response is required. This algorithm is based on the transforming the time signal to the frequency domain and the filter coefficient is updated on the frequency domain; details of the procedure have been summarised (Ferrara 1980).

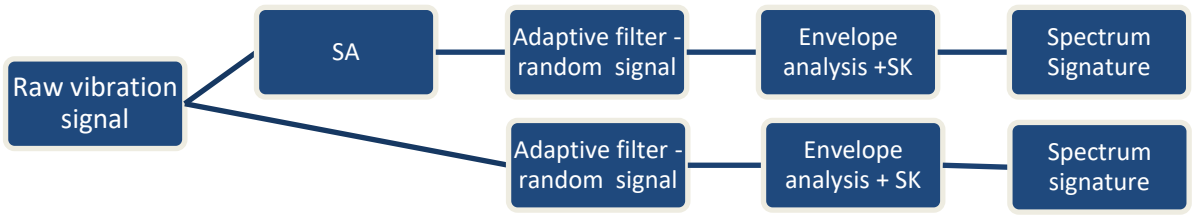

Figure 1 Schematic Signal Processing procedures

1.1 Synchronous Averaging

Synchronous Averaging (SA) technique is proven for analysis of machine vibration (McFadden, Toozhy 2000). The technique used to separate the noise or random parts from the signal. SA is performed using a signal phased-locked with the angular position of a shaft within the system, which can be the pulses from the shaft tachometer (such as a Hall sensor or optical encoder, where the time at which the tachometer signal crosses from low to high is called the zero crossing). The tachometer signal is used to divide the signal into segments. The number of points in each segment should be equal; therefore, interpolation is performed to extend the number of points in the segment. Then the segments are averaged (McFadden 1987, McFadden, Toozhy 2000, Bechhoefer, Kingsley 2009).

1.2 Adaptive filter

Adaptive filters are used to relate two vibration signals and produce a mathematical model for this correlation. The standard form of the adaptive filters is based on Wold

theory (Widrow, Glover et al. 1975) where the desired output estimated by multiplying the vibration signal by the filter coefficients, the filter coefficient are estimated iteratively based on the correlation between the vibration signal and reference signal. (Douglas 1999). Adaptive filters decompose the vibration into two signals based on equation 1(Douglas, Rupp 1999).

$$x(n) = P(n) + r\,(n) \tag{1}$$

In which P(n) is the gear signal

r(n) is the bearing signal

x(n) is the vibration signal

Prediction of the gear signal depends on the estimation of the filter coefficient . Many recursive algorithms have been suggested for filter coefficient optimisation. Among these algorithms, Least Mean Square LMS algorithm emerged as a good candidate. LMS compare the desired output to the reference signal and modify the filter coefficient accordingly. Such method requires the existence of reference signal and known as adaptive noise cancellation. Due to difficulty associate with obtaining a reference signal for bearing signal, the reference signal has been replaced by delayed version of the same signal (Widrow, Glover et al. 1975, Widrow, McCool et al. 1975).

LMS algorithm determines and update the coefficients for each filter step. Such process requires longer processing time, therefore Fast block Least Mean Square FBLMS has been suggested to overcome h the limitation of LMS (Dentino, McCool et al. 1978). In FBLMS the filter coefficient estimated for the signal spectrum and updated for each segment, details of application of FBLMS is summarised in (Ferrara 1980)

Spectral Kurtosis and envelope analysis

Kurtosis has been used as bearing health condition indicator for years. It is defined as the fourth standardised moment of the vibration signal, which present how peak or flat the distribution is. It is known that KU is a measure of the peakedness of a signal and on the basis that a signal will contain impulsive transient events during the onset of degradation. kurtosis value close to 3 indicates a Gaussian signal. Kurtosis greater than 3 indicates a sharp peak signal. As Short-Time-Frequency-Transform (STFT)

based (Randall 2011), SK measures impulsiveness of the signal in the different frequency band, thus the most impulsive frequency components which might contain fault signatures could be identified and extracted. SK has been extensively used in fault detection and condition monitoring. A very thorough definition and application of SK has been demonstrated by Antoni (Antoni 2007).

Spectral Kurtosis has been introduced to select the optimum frequency band for envelope analysis. In order to enhance efficiency in determining appropriate frequency resolution, Kurtogram is developed, which display SK as a function of both frequency and frequency resolution. In this way, an optimal band pass filter could be designed to extract signals with maximum impulsiveness in certain frequency bands and centre frequencies. Antoni has also suggested a fast kurtogram algorithm lessen the complicated computational work of kurtogram exploring the entire plane of frequency/ resolution (Antoni 2007).

Envelope analysis has been established as benchmark method for dealing with bearing fault diagnosis. The procedure of envelope analysis is described in (Elasha, Mba et al. 2014). It comprises of filtering the signal using frequency band obtained by SK, to form envelope signal, and then searching for desired frequency features.

One problem when applying envelope analysis is that selecting frequency bands for filtering might be challenging. Impacts due to defects could excite resonance at higher frequencies. With the aid of Kurtogram, it is possible to identify these structural resonance frequencies and filter them out subsequently.

The basic principle of this method is to calculate the Kurtosis at different frequency bands in order to identify non-stationarities in the signal and determine where they are located in the frequency domain. Obviously, the results obtained strongly depend on the width of the frequency bands Δf (Antoni 2007).

The Kurtogram (Randall 2011) is basically a representation of the calculated values of the SK as a function of f and Δf. However, the exploration of the whole plane (f, Δf) is a complicated computation task though Antoni (Antoni 2007) suggested a methodology for the fast computation of the SK.

On identification of the frequency band in which the SK is maximised, this information can be used to design a filter which extracts the part of the signal with the highest level of impulsiveness. Antoni et al. (Antoni, Randall 2006) demonstrated how the optimum filter which maximises the signal to noise ratio is a narrowband filter at the maximum value of SK. Therefore the optimal central frequency fc and bandwidth Bf of the band-pass filter are found as the values of f and Δf which maximise the Kurtogram. The filtrated signal can be finally used to perform an envelope analysis, which is a widely used technique for identification of modulating frequencies related to bearing faults. In this investigation, the SK computation and the subsequent signal filtration and envelope analysis were performed using the original Matlab code programmed by Jérôme Antoni (Antoni, Randall 2006).

2 Experimental Setup

Experimental data was obtained from tests performed on CS-29 Category 'A' helicopter gearbox which was seeded with defects in one of the planetary gears bearing of the second epicyclic stage. The test rig was of back-to-back configuration and powered by two motors simulating dual power input.

CS-29 'Category A' helicopter main gearbox

The transmission system of a CS-29 'Category A' helicopter gearbox is connected to two shafts, one from each of the two free turbines engines, which drive the main and tail rotors through the MGB. The input speed to the MGB is typically in the order of 23,000 rpm which is reduced to the nominal main rotor speed of 265 rpm [38].

The main rotor gearbox consists of two sections, the main module, which reduces the input shaft speed from 23,000 rpm to 2,400 rpm. This section includes two parallel gear stages. This combined drive provides power to the tail rotor drive shaft and the

bevel gear. The bevel gear reduces the rotational speed of the input drive to 2,405 rpm and changes the direction of the transmission to drive the epicyclic reduction gearbox module. The second section is the epicyclic reduction gearbox module which is located on top of the main module. This reduces the rotational speed to 265 rpm which drives the main rotor. This module consists of two epicyclic gears stage, the first stage contains 8 planets gears and second stage with 9 planets gears, see figure 2. The details of the gears are summarised in table 1.

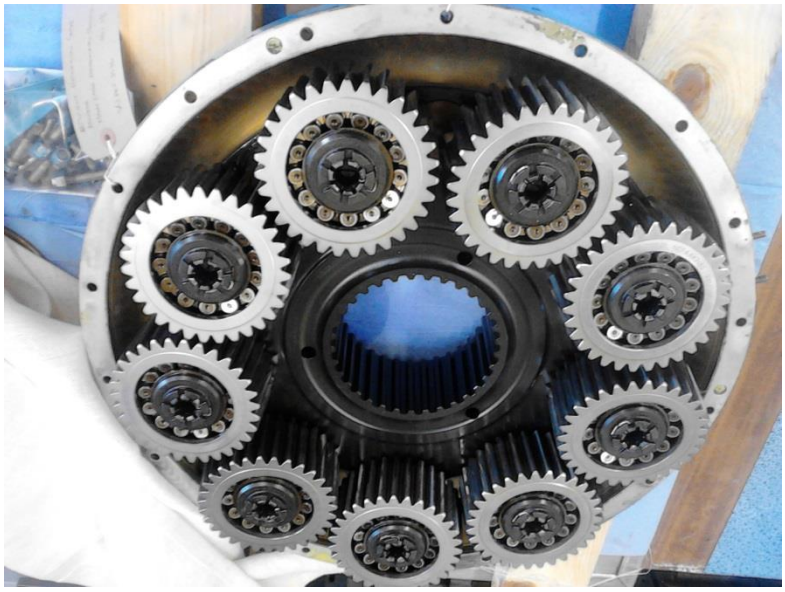

Figure 2 Second stage epicyclic gears

Table 1 number of teeth for the gearbox gears

First parallel stage	Pinion teeth	Wheel teeth	
	23	66	
Second parallel stage	Pinion teeth	Wheel teeth	
	35	57	
Bevel stage	Pinion teeth	Bevel teeth	
	22	45	
1st epicyclic stage	Sun gear	Planets gear – 8 gears	Ring gear
	62	34	130
2nd epicyclic stage	Sun gear	Planets gear – 9 gears	Ring gear
	68	31	130

The epicyclic module planet gears are designed as a complete gear and bearing assembly. The outer race of the bearing and the gear wheel are a single component,

with the bearing rollers running directly on the inner circumference of the gear. Each planet gear is ‘self-aligning’ by the use of spherical inner and outer races and barrel shaped bearing rollers (see Figure 2).

Experimental conditions and setup

This investigation involved performing the tests for fault-free condition, minor bearing damage and major bearing damage. The bearing faults were seeded on one of the planet gears of the second epicyclic stage. Minor damage was simulated by machining a rectangular section of fixed depth and width across the bearing outer race (10mm wide and 0.3mm deep), see figure 3, and the major damage simulated as a combination of both a damaged inner race (natural spalling around half of the circumference) and an outer race (about 30mm wide, 0.3mm deep), see figure 4. The load condition of 100% of maximum continuous power; the power, speed and torque characteristics of this load conditions are summarised in table 2.

Figure 3 Slot across the bearing outer race

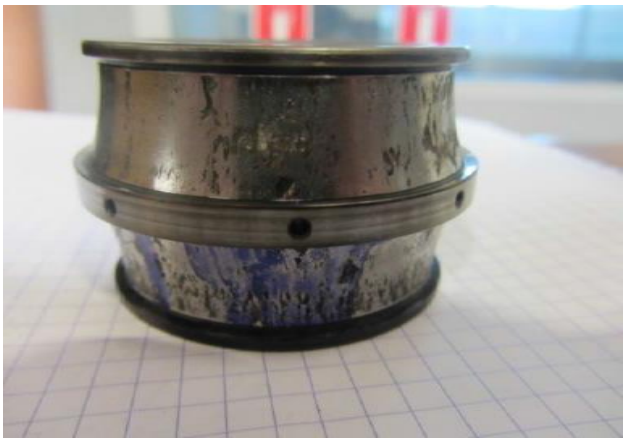

Figure 4 Inner race natural spalling

Table 2 Test Load conditions characteristics

Load Condition	Power (Kw)	Rotor speed (RPM)	Right input torque (Nm)	Left input torque Nm)
100% Max continuous power	1300	265	272	272

Vibration fault frequencies

To aid diagnosis all characteristic vibration frequencies were determined, see table 3. These included gears mesh frequencies of the different stages and the bearing defect frequencies for planet bearing.

Table 3 Gearbox characteristic frequencies

Frequency components	Frequency HZ
Gears Meshes	
First parallel GMF Hz	8751
Second parallel GMF	4641
Bevel stage GMF (Hz)	1791
1st epicyclic stage GMF	1671
2nd epicyclic stage GMF	573
Faulty planet bearing	
Ball spin	45
Outer race	97
Inner race	144
Cage	7.4

Data acquisition and instrumentation

Vibration data was acquired with a triaxial accelerometer (type PCB Piezotronics 356A03) at a sampling frequency of the 51.2 kHz. The accelerometer had an operating frequency range of 2 Hz to 8 kHz and was bonded to the case of the gearbox, see figure 5. The acquisition system employed was a National Instruments (NI) NI cDAQ-9188XT CompactDAQ Chassis. A 60 second sample was recorded for each fault case. The Y-axis of the tri-axial accelerometer arrangement was oriented parallel to the radial direction of gearbox, the X-axis to the tangential axis, and the Z-axis is the vertical axis parallel to the rotor axis, see figure 5. In addition, the angular position has been measured using a 60 segment encoder fitted to rotor (upper planet carrier), and sampled at 25.6 KHz.

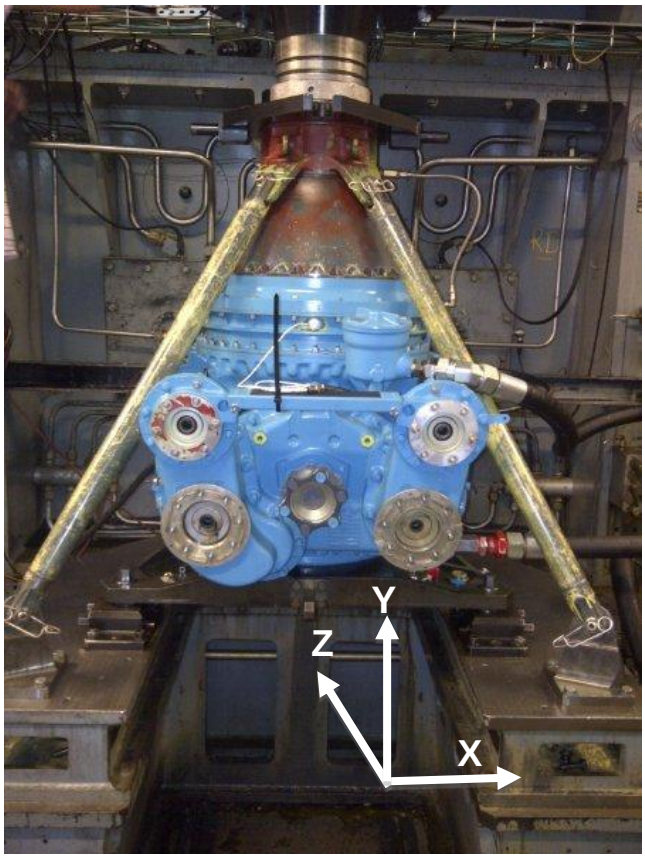

Figure 5 MGB installed on the test bench

3 Vibration analysis prior to TSA

The results of spectrum analysis show no evidence of bearing fault frequency for the faulty condition (Fig. 6). The spectrum showed the existence of gear mesh frequencies and their harmonic. In addition, observations of a closer inspection of the frequency spectrum (zoom in Fig. 7) showed no existence of the bearing fault frequency. When comparing all three test conditions, it was noted that the overall vibration amplitude decreased for the major fault scenario and this was due to the increased bearing clearance due the fault; a similar fault condition has been reported by Elasha et al. (2014b).

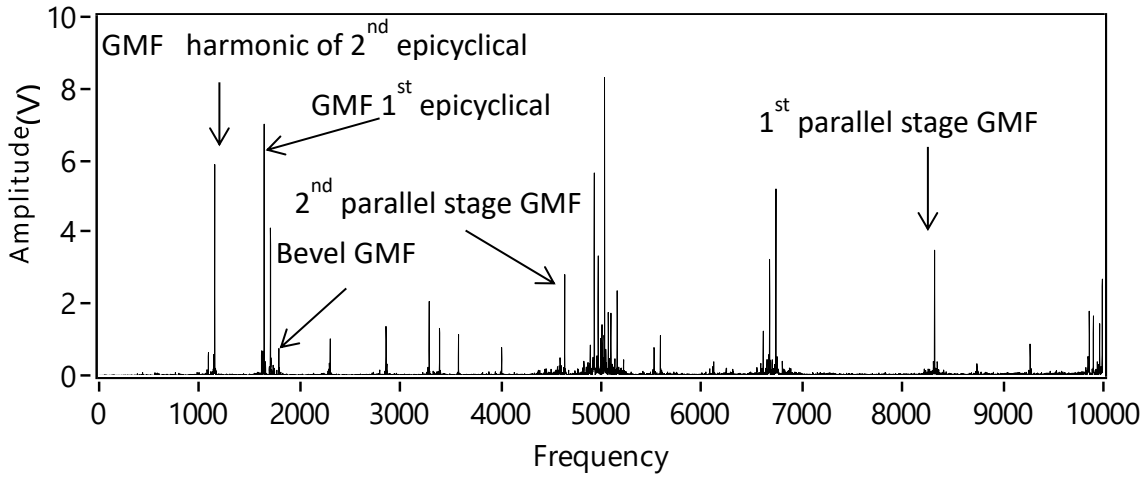

Figure 6 Power spectrum of original vibration signal for the major defect condition

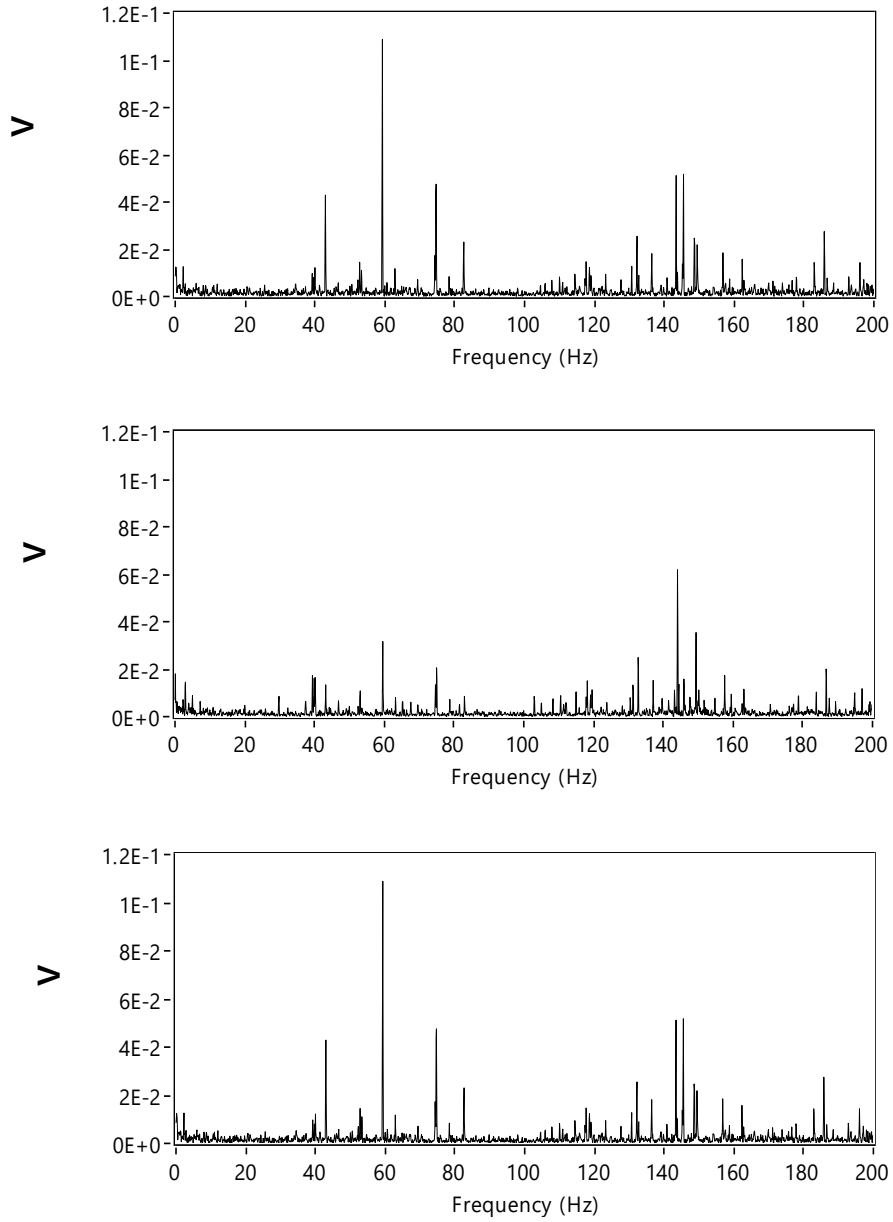

303

304

305

306 Figure 7 Zoom-in power spectrum of original vibration signal for a) Fault-free (b) Major
307 (c) Minor damage

308

309 Spectral Kurtosis analysis was undertaken on the non-deterministic part of data sets
310 collected from the gearbox for the different fault cases and this yielded the frequency
311 bands and center frequencies which were then used to undertake envelope analysis.
312 As discussed earlier the signal separation was undertaken with adaptive filter FBLMS
313 algorithm. Spectral plots of enveloped vibration signals following filtration, whose
314 characteristics were determined with the aid of Spectral Kurtosis, are show in figures
315 8, 9 and 10.

316

Table 4 Filter characteristics estimated based on combination indicator for all three vibration axes at 100% maximum take-off power

Case	Center frequency F_c (Hz)	Band Width Bw (Hz)	Kurtosis
Fault-free condition X direction	5200	266	0.1
Fault-free condition Y direction	5200	266	0.1
Fault-free condition Z direction	5200	266	0.11
Minor damage condition X direction	6000	266	0.11
Minor damage condition Y direction	6000	266	0.1
Minor damage condition Z direction	6000	266	0.12
Major damage condition X direction	20266	2133	0.5
Major damage condition Y direction	20266	2133	0.45
Major damage condition Z direction	20266	2133	0.6

Observation from the spectra of the enveloped signal in the all directions at 100% maximum continuous power, see figures 8, 9 and 10 respectively, showed no presence of fault frequencies associated with the defective planetary bearing in the spectrum, except for the Z direction, see Figure 10, where the cage defect frequency (7.5 Hz) were detected. It is apparent that the signal separation had not completely removed the gear mesh and shaft frequencies, particularly the sun gears frequencies and its harmonics for first and second epicyclic stages (38.8 and 13.2 Hz respectively), which were detected by envelope analysis, see figures 8, 9 and 10 respectively. Existence of these frequencies is due to fact that the vibration signal used in this analysis wasn't synchronised to any particular shaft. Observations at 110% of take-off power and 80% of maximum continuous power showed similar observation at 100% of maximum continuous power in all directions; therefore, only observation at 100% of maximum continuous power was presented here.

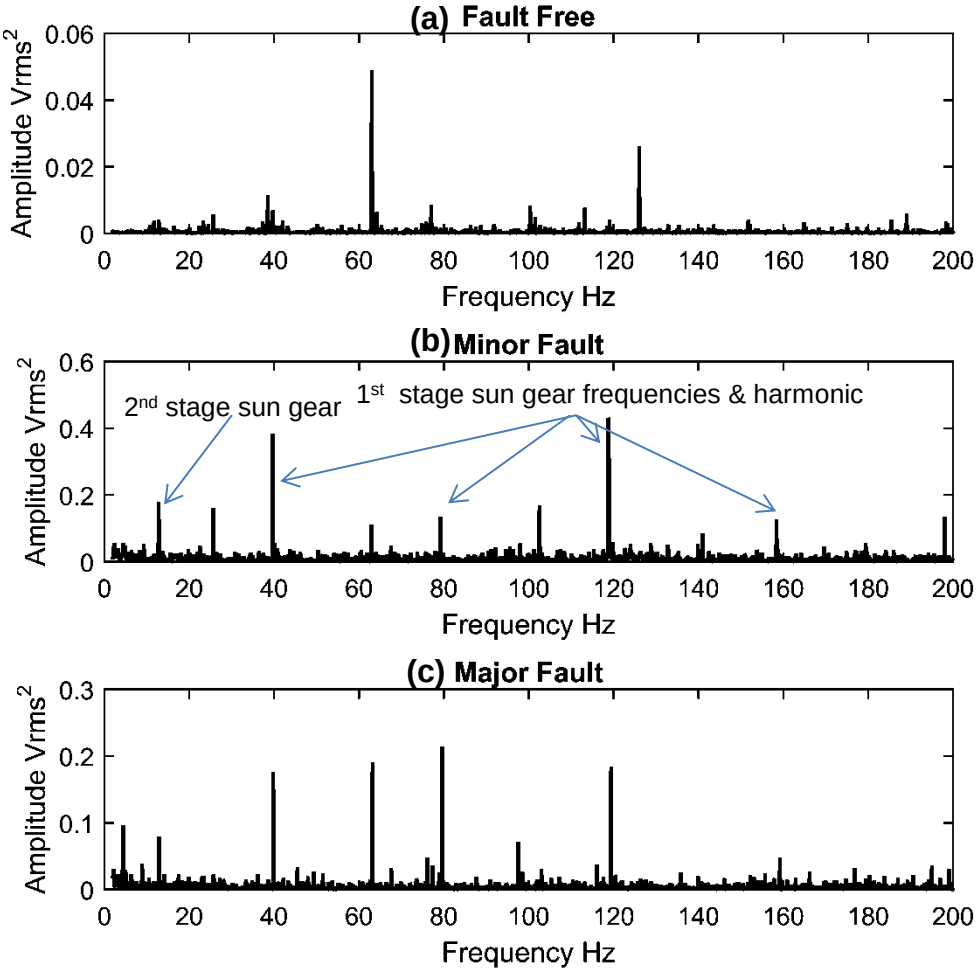

336

337

338 Figure 8 Enveloped Spectra of non-deterministic signal for a) Fault-free (b) Major (c)

339 Minor damage (100% maximum continuous power, X direction).

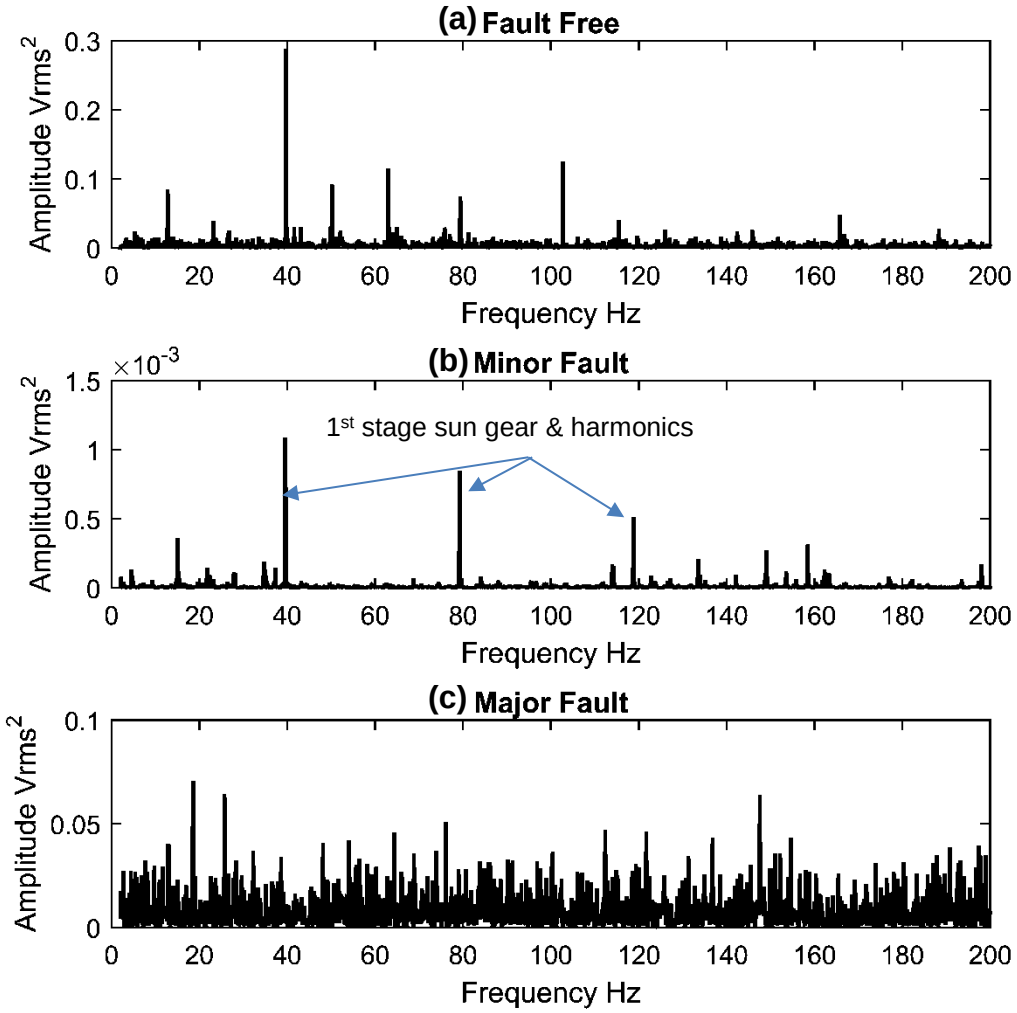

340

341 Figure 9 Enveloped Spectra of non-deterministic signal for a) Fault-free (b) Major

342 (c) Minor damage (100% of maximum continuous power, Y direction).

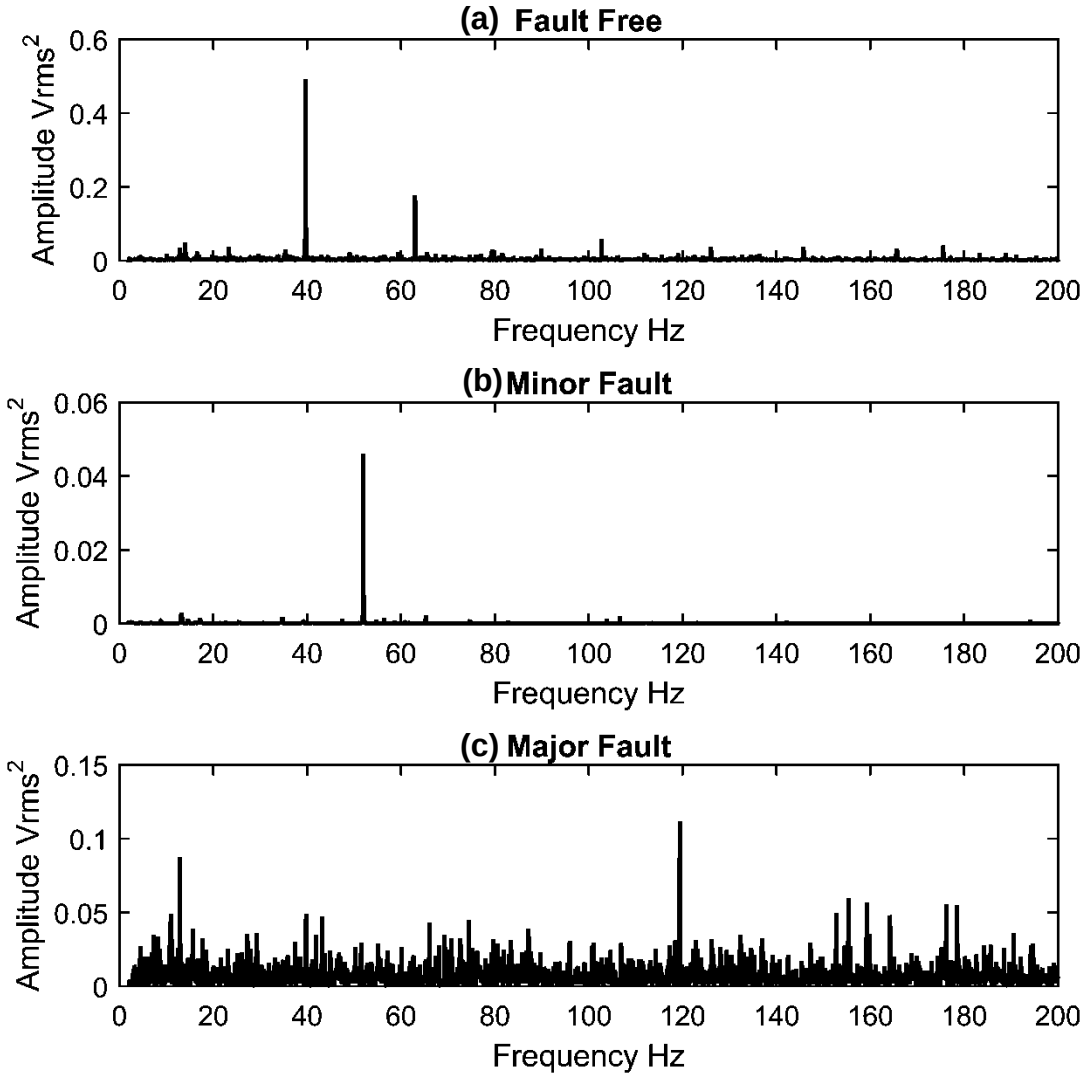

Figure 10 Enveloped Spectra of non-deterministic signal for a) Fault-free (b) Minor (c) Major damage (100% of maximum continuous power, Z direction)

4 Vibration analysis after SA

The vibration and tachometer signals acquired were processed to build the synchronous averaging signals, and then the non-deterministic part of TSA signal has been obtained using adaptive signal separation as descried earlier. Spectrum analysis of the separated signal showed no indication of the bearing failure, therefore, the signal processed further using envelope analysis, and the frequency bands required

for envelope analysis have been obtained using spectral kurtosis analysis. In order to detect the faults all related frequencies have been estimated as orders of rotor speed (265 RPM), see Table 5.

Table 5: Frequencies in orders of rotor rotation

Frequency components	**Order (of rotor speed 265 RPM)**
Gears Meshes	
First parallel GMF Hz	1982.7
Second parallel GMF	1050
Bevel stage GMF (Hz)	405
1st epicyclic stage GMF	378.33
2nd epicyclic stage GMF	129.73
Faulty planet bearing	
Ball spin	10.25
Outer race	21.9
Inner race	32.6
Cage	1.7

Observation from the spectra of the enveloped signal in the X direction at 100% maximum take-off power, see Figure 11, showed existence of outer race defect frequency (21.9 orders) for both minor and major faults. In addition, inner race defect has been detected for the major fault condition at 32.6 orders. Also, second harmonic of outer race (43.8 orders) has been detected for the minor fault.

Observations from envelope spectra in the Y and Z direction at 100% maximum take-off power, see Figure 12 and Figure 13, showed existence outer race defect frequency for major fault condition. Furthermore, outer race defect has been identified for the minor fault detection in Y direction, however, observations of Z direction showed no fault existence, see Figure 13.

370

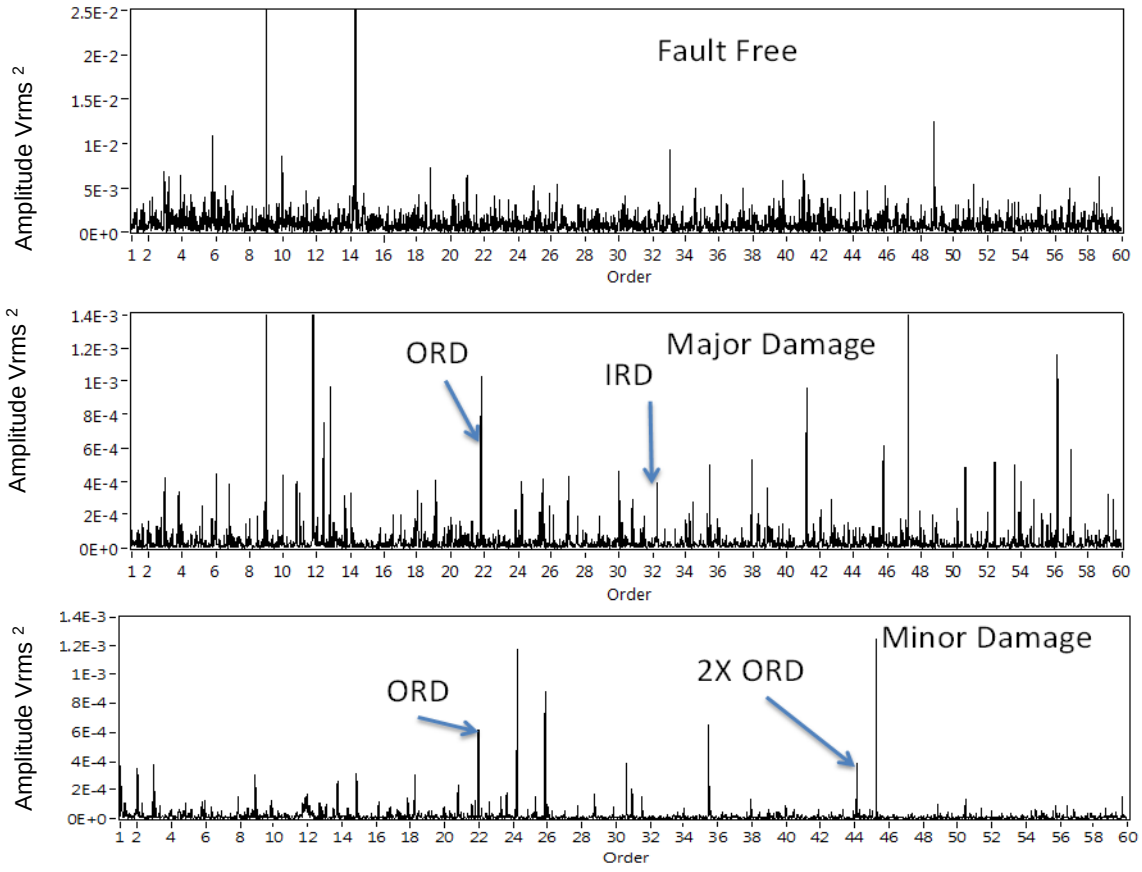

371

372 Figure 11 Enveloped Spectra of TSA non-deterministic signal for a) Fault-free (b)
373 Major (c) Minor damage (100% maximum continuous power, X direction).

374

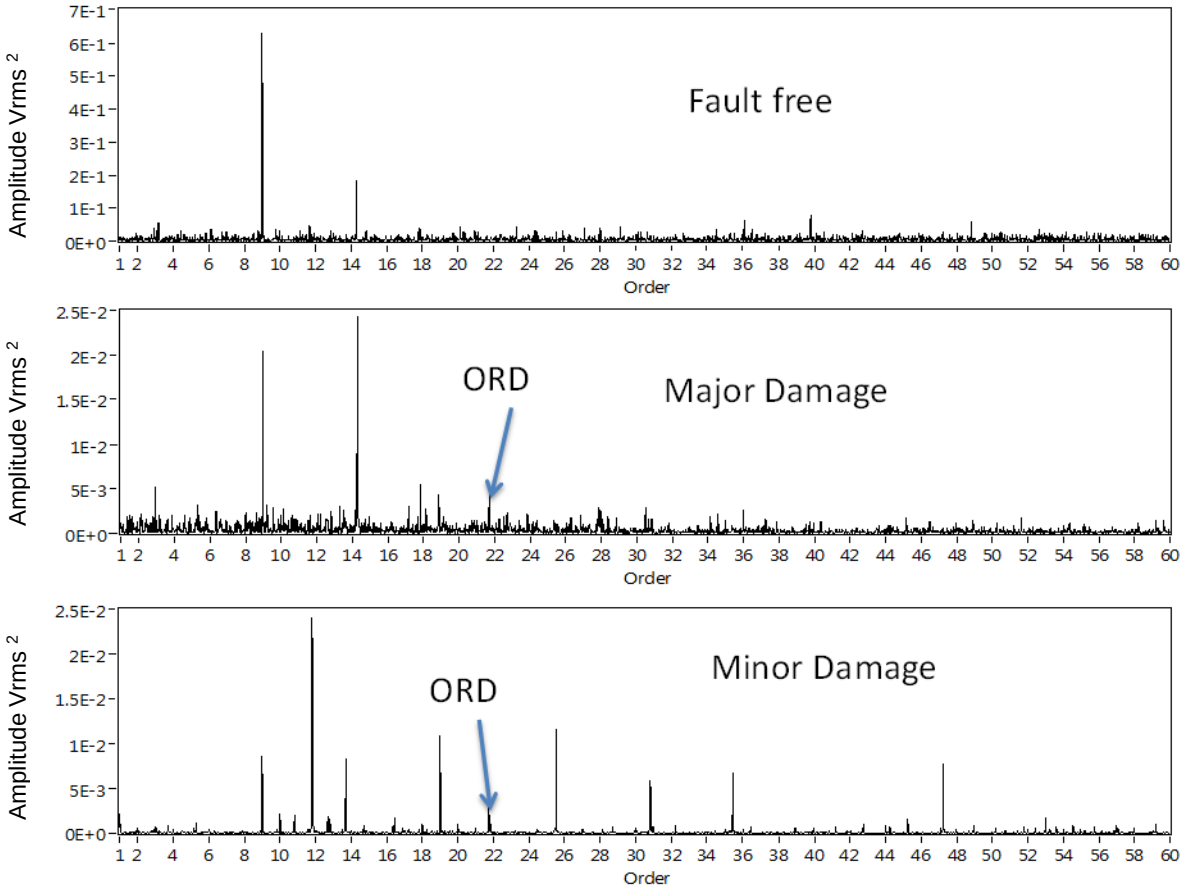

375

376 Figure 12 Enveloped Spectra of TSA non-deterministic signal for a) Fault-free (b)
377 Major (c) Minor damage (100% maximum continuous power, Y direction).

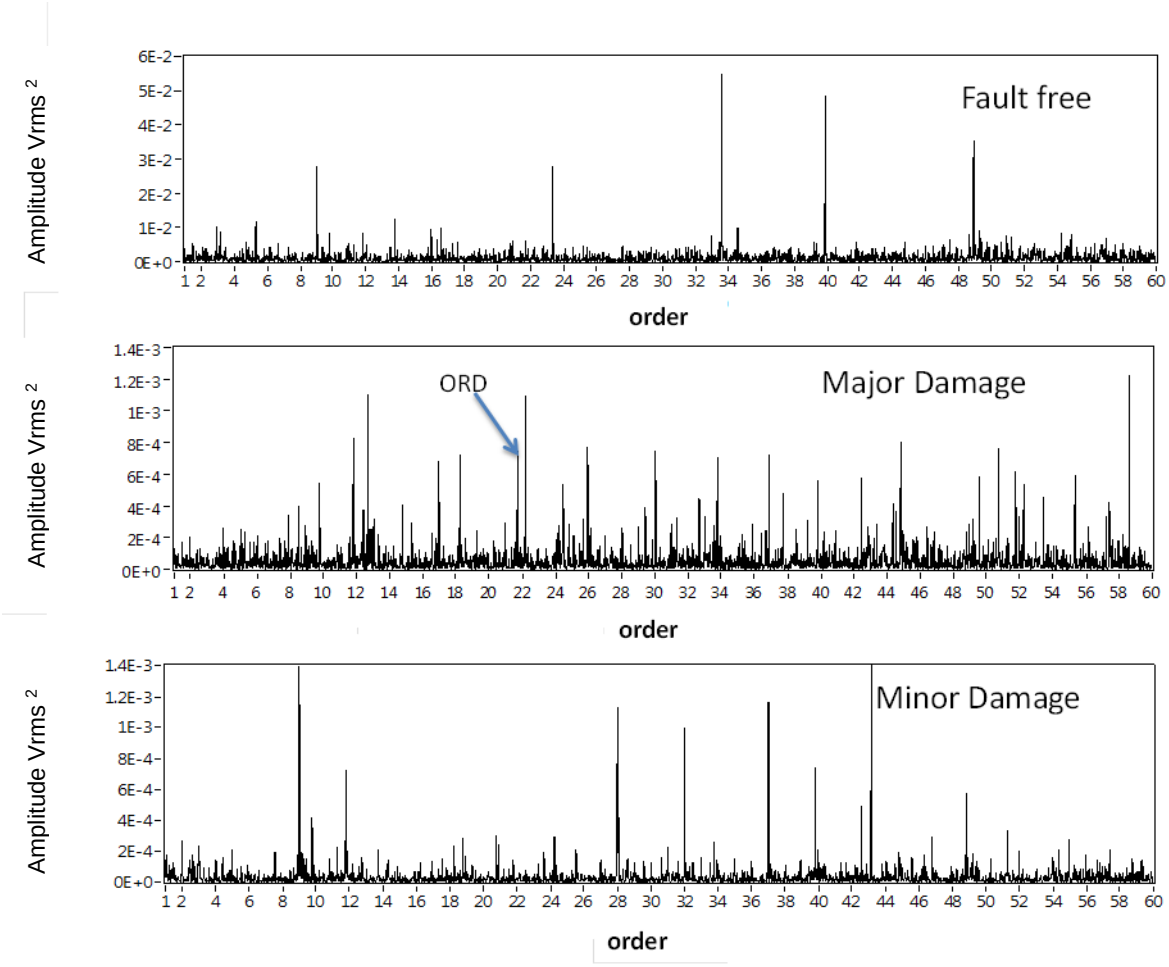

Figure 13 direction Enveloped Spectra of TSA non-deterministic signal for a) Fault-free (b) Major (c) Minor damage (100% maximum continuous power, Z direction).

5 Discussion and Conclusion

Comparisons of the vibration results prior to and after application of TSA showed the superiority of TSA in improving the signal separation performance, leading to detection of the bearing faults for both minor and major fault conditions. The results prior to application of the TSA technique showed no fault existence. Though the results after TSA showed sensitivity to measurement direction and load condition, the result of measurement taken under minor

fault for the z-direction showed the existence of no faults for all loading conditions, where the measurements taken in the x- and y-directions showed the existence of the minor fault.

The applied signal processing techniques were able to aid identification of the planetary module bearing fault using signal separation and SK to optimize envelope analysis.

In summary, this research recommends employing of series of signal processing techniques to detect the bearing fault within helicopter gearboxes using vibration analysis. Application of these techniques results in bearing fault identification for different defect sizes and under different loading condition. Finally, application of TSA prior to vibration signal separation offered a clearer indication of damage than vibration signal separation without employing

of TSA.

Acknowledgements

This work was conducted as part of EASA study 2015.OP.13 into improved detection techniques for helicopter main gearbox defects.

References

[1] Cotrell, J. R. (2002), "A preliminary evaluation of a multiple-generator drivetrain configuration for wind turbines", *ASME 2002 Wind Energy Symposium,* American Society of Mechanical Engineers, pp. 345.

[2] McFadden, P. D. (1987), "A revised model for the extraction of periodic waveforms by time domain averaging", *Mechanical Systems and Signal Processing,* vol. 1, no. 1, pp. 83-95.

[3] Samuel, P. D. and Pines, D. J. (2005), "A review of vibration-based techniques for helicopter transmission diagnostics", *Journal of Sound and Vibration,* vol. 282, no. 1–2, pp. 475-508.

[4] McFadden, P. D. and Toozhy, M. M. (2000), "Application of Synchronous Averaging to Vibration Monitoring of rolling elements bearings", *Mechanical Systems and Signal Processing,* vol. 14, no. 6, pp. 891-906.

[5] Wang, W. (2001), "Early detection of gear tooth cracking using the resonance demodulation technique", *Mechanical Systems and Signal Processing,* vol. 15, no. 5, pp. 887-903.

[6] Sawalhi, N., Randall, R. B. and Forrester, D. (2014), "Separation and enhancement of gear and bearing signals for the diagnosis of wind turbine transmission systems", *Wind Energy,* vol. 17, no. 5, pp. 729-743.

[7] McFadden, P. D. and Smith, J. D. (1984), "Vibration monitoring of rolling element bearings by the high-frequency resonance technique — a review", *Tribology International,* vol. 17, no. 1, pp. 3-10.

[8] Yang, W., Tavner, P. J. and Wilkinson, M. R. (2009), "Condition monitoring and fault diagnosis of a wind turbine synchronous generator drive train", *Renewable Power Generation, IET,* vol. 3, no. 1, pp. 1-11.

[9] Wenxian Yang, Tavner, P. J., Crabtree, C. J. and Wilkinson, M. (2010), "Cost-Effective Condition Monitoring for Wind Turbines", *Industrial Electronics, IEEE Transactions on,* vol. 57, no. 1, pp. 263-271.

[10] Randall, R. B., Sawalhi, N. and Coats, M. (2011), "A comparison of methods for separation of deterministic and random signals", *The International Journal of Condition Monitoring,* vol. 1, no. 1, pp. 11.

[11] Randall, R. B. and Antoni, J. (2011), "Rolling element bearing diagnostics—A tutorial", *Mechanical Systems and Signal Processing,* vol. 25, no. 2, pp. 485-520.

[12] Antoni, J. and Randall, R. B. (2001), "optimisation of SANC for Separating gear and bearing signals", *Condition monitoring and diagnostics engineering management,* , no. 1, pp. 89-99.

[13] Randall, R. B. (2004), "Detection and diagnosis of incipient bearing failure in helicopter gearboxes", *Engineering Failure Analysis,* vol. 11, no. 2, pp. 177-190.

[14] Ho, D. and Randall, R. B. (2000), "Optimisation of bearing diagnostic techniques using simulated and actual bearing fault signal", *Mechanical Systems and Signal Processing,* vol. 14, no. 5, pp. 763-788.

[15] Antoni, J. (2005), "Blind separation of vibration components: Principles and demonstrations", *Mechanical Systems and Signal Processing,* vol. 19, no. 6, pp. 1166-1180.

[16] Li, Z., Yan, X., Tian, Z., Yuan, C., Peng, Z. and Li, L. (2013), "Blind vibration component separation and nonlinear feature extraction applied to the nonstationary vibration signals for the gearbox multi-fault diagnosis", *Measurement,* vol. 46, no. 1, pp. 259-271.

[17] Barszcz, T. (2009), "Decomposition of vibration signals into deterministic and nondeterministic components and its capabilities of fault detection and identification", *International Journal of Applied Mathematics and Computer Science,* vol. 19, no. 2, pp. 327-335.

[18] Randall, R. B. (2011), *Vibration-based Condition Monitoring,* first ed, John Wiley and sons Ltd, UK.

[19] Wang, W. (2008), "Autoregressive model-based diagnostics for gears and bearings", *Insight-Non-Destructive Testing and Condition Monitoring,* vol. 50, no. 8, pp. 414-418.

[20] Makhoul, J. (1975), "Linear prediction: A tutorial review", *Proceedings of the IEEE,* vol. 63, no. 4, pp. 561-580.

[21] Satorius, E. H., Zeidler, J. R. and Alexander, S. T. (1979), "Noise cancellation via linear prediction filtering", *Acoustics, Speech, and Signal Processing, IEEE International Conference on ICASSP '79.* Vol. 4, pp. 937.

[22] Thakor, N. V. and Zhu, Y. (1991), "Applications of adaptive filtering to ECG analysis: noise cancellation and arrhythmia detection", *Biomedical Engineering, IEEE Transactions on,* vol. 38, no. 8, pp. 785-794.

[23] Chaturved, G. K. and Thomas, D. W. (1981), "Adaptive noise cancelling and condition monitoring", *Journal of Sound and Vibration,* vol. 76, no. 3, pp. 391-405.

[24] Antoni, J. and Randall, R. B. (2004), "Unsupervised noise cancellation for vibration signals: part I—evaluation of adaptive algorithms", *Mechanical Systems and Signal Processing,* vol. 18, no. 1, pp. 89-101.

[25] Widrow, B., Glover, J. R., Jr., McCool, J. M., Kaunitz, J., Williams, C. S., Hearn, R. H., Zeidler, J. R., Eugene Dong, J. and Goodlin, R. C. (1975), "Adaptive noise cancelling: Principles and applications", *Proceedings of the IEEE,* vol. 63, no. 12, pp. 1692-1716.

[26] Simon, H. (1991), *Adaptive Filter theory,* Second ed, Prentice-Hall international, Inc, USA.

[27] Ruiz-Cárcel, C., Hernani-Ros, E., Cao, Y. and Mba, D. (2014), "Use of Spectral Kurtosis for Improving Signal to Noise Ratio of Acoustic Emission Signal from Defective Bearings", *Journal of Failure Analysis and Prevention,* vol. 14, no. 3, pp. 363-371.

[28] Antoni, J. and Randall, R. (2006), "The spectral kurtosis: application to the vibratory surveillance and diagnostics of rotating machines", *Mechanical Systems and Signal Processing,* vol. 20, no. 2, pp. 308-331.

[29] Antoni, J. (2007), "Fast computation of the kurtogram for the detection of transient faults", *Mechanical Systems and Signal Processing,* vol. 21, no. 1, pp. 108-124.

[30] Dwyer, R. (1983), "Detection of non-Gaussian signals by frequency domain kurtosis estimation", *Acoustics, Speech, and Signal Processing, IEEE International Conference on ICASSP'83.* Vol. 8, IEEE, pp. 607.

[31] Elasha, F., Ruiz-Carcel, C., Mba, D. and Chandra, P. (2014), "A Comparative Study of the Effectiveness of Adaptive Filter Algorithms, Spectral Kurtosis and

Linear Prediction in Detection of a Naturally Degraded Bearing in a Gearbox", *Journal of Failure Analysis and Prevention,* vol. 14, no. 5, pp. 623-636.

[32] Dentino, M., McCool, J. and Widrow, B. (1978), "Adaptive filtering in the frequency domain", *Proceedings of the IEEE,* vol. 66, no. 12, pp. 1658-1659.

[33] Ferrara, E. R. (1980), "Fast implementations of LMS adaptive filters", *Acoustics, Speech and Signal Processing, IEEE Transactions on,* vol. 28, no. 4, pp. 474-475.

[34] Bechhoefer, E. and Kingsley, M. (2009), "A review of time synchronous average algorithms", *Annual Conference of the Prognostics and Health Management Society, San Diego, CA, Sept,* pp. 24.

[35] Douglas, S. C. (1999), *Introduction to Adaptive Filters,* CRC Press.

[36] Douglas, S. C. and Rupp, M. (1999), "Convergence Issues in the LMS Adaptive Filter", in Madisetti, V. K. (ed.) *The Digital signal processing handbook,* Second ed, CRC press, Atlanta, USA.

[37] Widrow, B., McCool, J. and Ball, M. (1975), "The complex LMS algorithm", *Proceedings of the IEEE,* vol. 63, no. 4, pp. 719-720.

[38] Department for Transport (2011), *Report on the accident to aerospatiale (Eurrocopter) AS332 L2 Super Puma,registration G-REDL 11 nm NE of Peterhead, Scotland, on 1 April 2009 ,* 2/2011, Air Accident Investigation Branch, Aldershot, UK.